Test-Analysis Correlation of the Space Shuttle Solid Rocket Motor Center Segment

Daniel C. Kammer*
SDRC, Inc., San Diego, California
and
Brent M. Jensen† and Donald R. Mason‡
Morton Thiokol, Inc., Brigham City, Utah

Modal surveys of inert and live Space Shuttle solid rocket booster center segments were performed to characterize the dynamic properties of the motor case and solid propellant grain. Advanced pretest analysis techniques were used to determine accelerometer locations and generate exact reduced representations of the analytical models to be used in test-analysis correlation. Following the modal surveys, the analytical models were quickly updated using design sensitivity and optimization techniques to provide an accurate analytical representation after only a few iterations. The elastic modulus for both the inert and live solid propellant was increased substantially from predicted pretest values. Correlation of the inert segment required the elastic modulus to be increased by a factor of 4.67 over the value predicted by a rheometric dynamic spectrometer (RDS). Correlation of the live segment required an axial propellant modulus gradient. When RDS testing was performed at appropriate dynamic strain levels, results were found to be consistent with the modal survey.

Introduction

FAILURE of the Space Shuttle and Titan 34D solid rocket motors (SRM) has led to a renewed interest in the accuracy of analytical representations used for their dynamic analysis. Detailed finite-element models (FEM), such as the one pictured in Fig. 1, have been generated to investigate the static and dynamic response of the Space Shuttle solid rocket booster (SRB). Although greater FEM detail will in general lead to more accurate numerical results, errors will always exist due to uncertainties in the characterization of joint, physical, and material properties.

The dynamic characteristics of the solid propellant have been of particular interest to analysts. Propellant properties such as elastic modulus are not well known because of their nonlinear dependence on excitation frequency, strain level, and temperature. In addition, propellant is difficult to analyze due to its viscoelastic and incompressible nature. Therefore, past analyses have often ignored propellant dynamic effects. In many cases, propellant mass has been distributed either along the length of beam models or on the surface of the SRM case in shell representations, whereas propellant stiffness has been totally ignored.

The Space Shuttle SRB is constructed in four segments: a forward segment, two center segments, and an aft segment. Each SRB segment is constructed of two cylindrical steel case sections connected at a factory joint. The steel case surrounds a thick hollow cylinder of solid propellant that is continuous through the length of the segment. The propellant bore is tapered such that the mandrel used to form the bore can be easily removed. For example, the propellant bore diameter for a center segment varies almost 6.0 in. over its 320.0-in. length. Because of the extreme size and weight of the SRB, the segments are attached to each other at the launch site using field joints. Field joints differ from factory joints in that the propellant is continuous across a factory joint but discontinuous across a field joint.

To characterize the dynamic properties of the solid propellant and the steel case of the Space Shuttle SRB more accurately, modal survey tests of SRM center segments containing live and inert propellant were conducted at Morton Thiokol in January 1987. The inert segment test was performed first to verify methods and to resolve any safety issues regarding the vibration of a live center segment. The live segment test then followed. Results from the modal surveys were to be compared to the predictions of analytical models in which the propellant stiffness was characterized using premodal survey subscale propellant tests. Based on the results of the test-analysis correlation, the analytical representations would be corrected to predict the test modal parameters more accurately. A correlation between the results of the modal surveys and the subscale propellant tests was also desired.

This paper briefly discusses pretest analysis and modal survey results. The main topic of this work is a method of system identification that uses design sensitivity and optimization techniques[1,2] to adjust analytical models and its application to the inert and live center segment representations. This work represents an original application of design sensitivity and optimization techniques to the validation of an analytical

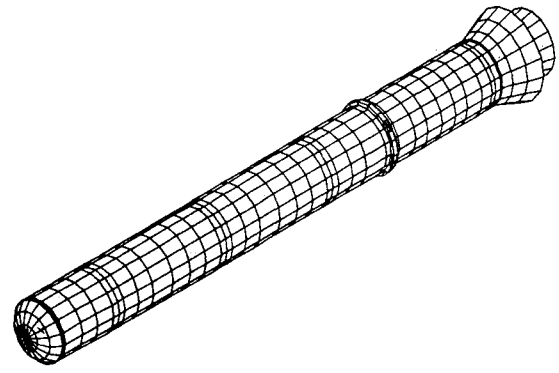

Fig. 1 Detailed finite-element representation of Space Shuttle solid rocket booster.

Received March 7, 1988; presented as Paper 88-2398 at the AIAA/ASME/ASCE/AHS 29th Structures, Structural Dynamics, and Materials Conference, Williamsburg, VA, April 21-22, 1988; revision received Dec. 13, 1988. Copyright © 1988 American Institute of Aeronautics and Astronautics, Inc. All rights reserved.

*Senior Project Engineer; currently Assistant Professor, Department of Engineering Mechanics, University of Wisconsin-Madison, WI. Member AIAA.
†Associate Scientist. Member AIAA.
‡Supervisor of Dynamics. Associate Fellow AIAA.

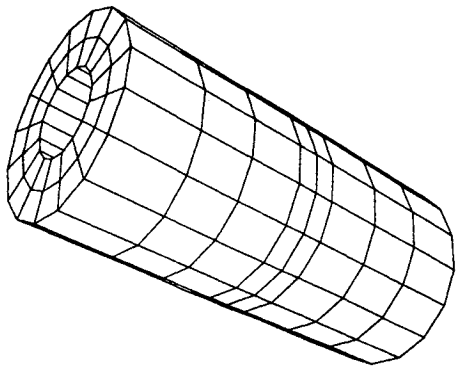

Fig. 2 Finite-element representation of solid rocket motor center segment.

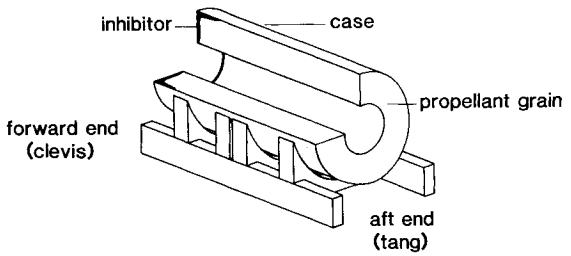

Fig. 3 Cutaway view of center segment in test suspension.

Table 1 Comparison of modal frequencies for pretest inert and live center segment analytical representations

Mode	Live segment Frequency, Hz	Inert segment Frequency, Hz	Description
1	0.844	0.869	First rigid-body roll
2	0.941	0.948	First rigid-body pitch
3	1.296	1.313	Rigid-body yaw
4	1.470	1.488	Rigid-body bounce
5	1.785	1.798	Second rigid-body pitch
6	2.247	2.265	Second rigid-body roll
7	5.114	8.583	Case-propellant aft ovaling
8	5.150	8.604	Case-propellant aft ovaling
9	5.303	8.855	Case-propellant forward ovaling
10	5.343	8.877	Case-propellant forward ovaling
11	10.482	17.703	Case-propellant aft triangular
12	10.510	17.719	Case-propellant aft triangular
13	10.892	18.159	Case-propellant forward triangular
14	10.919	18.175	Case-propellant forward triangular
15	11.520	19.712	Propellant symmetric axial
16	11.695	20.021	Propellant forward first-order shear
17	11.695	20.021	Propellant forward first-order shear
18	12.072	20.713	Propellant aft first-order shear
19	12.072	20.714	Propellant aft first-order shear
20	13.751	23.230	Live: propellant second-order shear/ Inert: case-propellant saddle

model of a loaded SRB segment. Advantages and disadvantages of this method will be discussed. The relation between the propellant dynamic modulus information extracted during the test-analysis correlation process and the modulus determined using subscale testing techniques also will be addressed.

Pretest Analysis

Before the modal survey, a finite-element model, illustrated in Fig. 2, was generated for the inert and live SRM center segments. The FEM's consisted of a thick-walled hollow cylinder of solid propellant modeled by linear solid elements[3] surrounded by a thin steel casing measuring 0.48 in. thick with a midplane diameter of 146 in. modeled using linear shell elements. The segment was supported using soft springs to model

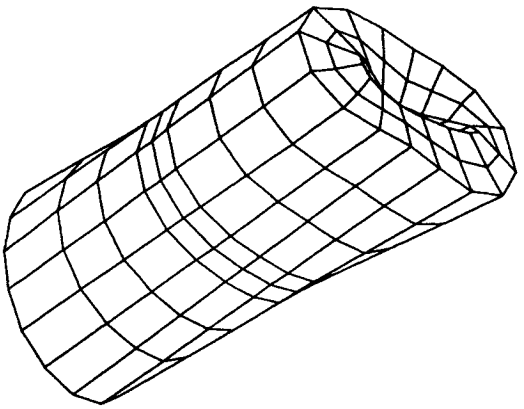

Fig. 4 Typical center segment case/propellant mode shape.

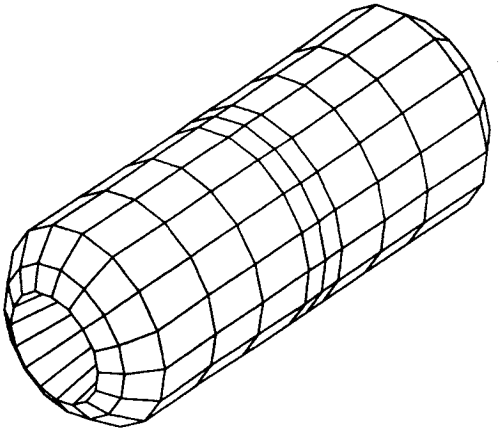

Fig. 5 Typical center segment propellant mode shape.

the test suspension system, illustrated in Fig. 3, which was used to represent free-free boundary conditions during the modal surveys. Model refinement studies were performed to determine the amount of detail required for the frequency range of interest.

A rheometric dynamic spectrometer (RDS) was used to measure the dynamic properties, storage modulus G', and loss modulus G'' of a small propellant specimen. The elastic modulus E was then computed from the measured storage modulus. Pretest measurements indicated that the elastic modulus was approximately 1000 psi for young live propellant and 3000 psi for aged inert propellant. These values were used in the corresponding pretest FEM representations.

Mode shapes and frequencies were computed for both the inert and live propellant center segment models. Table 1 compares the first 20 analytical inert and live segment modal frequencies. The first six modes represent rigid body motion in which the segment rigidly bounces on the test configuration suspension. The next eight mode shapes are case-propellant modes in which both the case and propellant participate, as illustrated in Fig. 4. Note that a small frequency difference exists between pairs of mode shapes involving deformation in the forward and aft portions of the segment because the segment is not axially symmetric. Modes 15–20 are propellant modes possessing very little case deformation. A typical propellant mode shape is shown in Fig. 5. Figure 6 presents the fraction of the total strain energy associated with the solid propellant for the inert segment mode shapes listed in Table 1. It is obvious from the figure that the propellant dominates the elastic body mode shape response, indicating that an accurate representation of the solid propellant grain is vital to an accurate FEM.

A correlation analysis was performed between analytical mode shapes for a center segment in a free-free configuration and analytical mode shapes for a center segment in the de-

scribed test configuration. A comparison of modal frequencies showed that the frequency of the fundamental elastic mode was increased 3.50% by the analytical representation of the test suspension. A comparison of the free-free and test-configuration mode shapes was made using a cross-orthogonality computation.[4] The cross-orthogonality matrix $[C]$ is computed using the expression

$$[C] = [\Phi_{\text{free}}]^T [M] [\Phi_{TC}] \quad (1)$$

where $[\Phi_{\text{free}}]$, $[M]$, and $[\Phi_{TC}]$ represent the free-free modes, the mass matrix, and the test-configuration mode shapes, respectively. The diagonal terms, called cross-generalized mass values, indicate the degree of correlation between the two sets of mode shapes used in the computation. Off-diagonal terms indicate the degree of orthogonality of the two mode sets. The computation for the free-free and test-configuration mode shapes produced a minimum cross-generalized mass value of 0.943 corresponding to the mass normalized fundamental elastic mode. A value of 1.00 would indicate that the free-free and test-configuration mode shapes were exactly equal. These correlation results indicate that the test suspension has only a small effect on the elastic mode shapes and frequencies and that it therefore correctly represents the desired free-free boundary condition.

Test and analysis modal parameters were compared using reduced representations of the inert and live segment FEM's called test-analysis models (TAM's). A TAM possesses a degree of freedom for each accelerometer location used in the modal survey. The TAM generation process optimizes the system of accelerometers used in the modal survey by minimizing the required number while maximizing the amount of independent test data gathered. The TAM's were developed using methods presented in Refs. 4 and 5. The modal reduction method of Ref. 5 produced TAM's that were exact representations of the original finite-element models in the frequency range of interest, thus eliminating all TAM generation error from the test-analysis correlation. This particular reduction method was vital to the generation of an accurate TAM representation of an SRM. Because of the propellant's high mass and low stiffness characteristics, the Guyan reduction, which has been used in the past for TAM generation, was totally inadequate.[5]

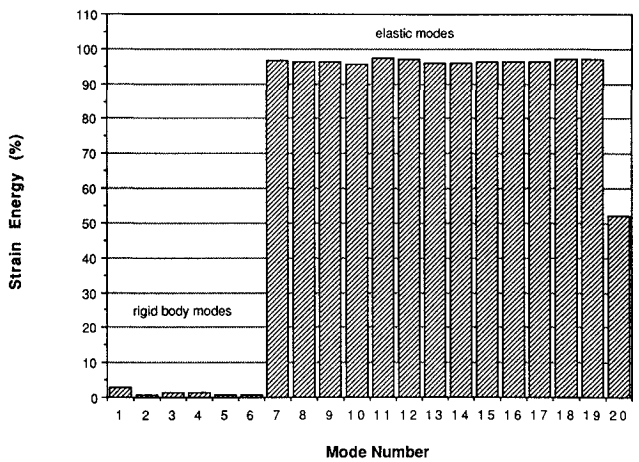

Fig. 6 Percentage of strain energy in propellant for inert center segment analytical mode shapes.

Modal Survey Results

During the modal survey, the segments were oriented horizontally in the rotator deck illustrated in Fig. 3. The segments were supported by a series of airbags at each of the four chocks to simulate a free-free boundary condition. Segment excitation was performed at three locations on the motor case: radially at the aft end, obliquely, and axially at the forward end. An axial exciter was also used on the propellant face during the inert segment modal survey. For safety reasons, no propellant excitation was performed during the live segment test.

Inert and live center segment response data was obtained using 230 accelerometers at 136 different locations, including 64 on the segment case, 16 on the end propellant faces, and 56 inside the segment along the propellant bore. During the inert segment test, 16 of the 56 propellant bore accelerometers were actually located in holes drilled deep into the propellant grain. Test data was collected using both multipoint random[6] and multiphased stepped sine[7] excitation methods. Real normal modes and complex modes were extracted using the direct parameter estimation technique described in Ref. 8. Details of the modal survey can be found in Ref. 9.

Ten test modes were extracted with frequencies below 45 Hz for the inert segment, and 11 test modes were found in this frequency range for the live segment. Table 2 compares the results of the inert and live modal surveys. A comparison of Tables 1 and 2 illustrates that there are large discrepancies between analysis and test modal frequencies. Therefore, the analytical models must be corrected through system identification techniques. It is also interesting to note that there is a 2.1-Hz frequency separation between the forward and aft ovaling modes in the live segment survey results. This frequency separation does not exist in either the inert segment test data or the analytical data.

Discussion of System Identification Methods

There are two basic approaches to the correction of a finite-element model based on test data. The first approach, direct matrix identification, adjusts the elements of the FEM mass and stiffness matrices so that they accurately predict the test modes and frequencies. Several methods using this approach

Table 2 Summary of inert and live center segment modal survey resutls

Inert segment		Live segment		
Frequency, Hz	Damping, C/Cr	Frequency, Hz	Damping, C/Cr	Description
2.14	14.8	1.94	13.9	First rigid-body pitch
3.32	5.2	3.20	6.8	Rigid-body bounce
4.14	3.5	3.76	7.1	Second rigid-body pitch
5.00	3.5	4.75	3.6	Second rigid-body roll
18.68	17.2	14.65	21.0	Case-propellant forward ovaling
18.81	16.1	16.73	17.4	Case-propellant aft ovaling
28.98	9.0	28.16	9.7	Case-propellant saddle
		28.13	17.7	Case-propellant saddle
40.87	13.9	38.63	21.0	Case-propellant forward triangular
41.52	11.8			Propellant
		40.16	18.9	Case-propellant second-order saddle
42.49	9.7	44.71	6.0	Case-propellant bending

have been developed in recent years.[10-14] Baruch and Bar Itzhack[10] were the first to use direct matrix identification to correct the analytical stiffness matrix based on constrained minimization theory. Berman[11] then extended Baruch's method to the correction of the analytical mass matrix. The resulting corrected mass and stiffness matrices exactly predict the test modes and frequencies. Kabe[13] and Kammer[14] modified the Baruch-Berman approach to include relative correction of the terms in the stiffness matrix and to account for the FEM connectivity.

Direct matrix identification methods such as the Baruch-Berman method were not used extensively because of the global nature of most of the FEM input parameters that possessed a high degree of uncertainty such as propellant modulus. Experience in the application of the Baruch-Berman method gained during the correlation of the segment models indicates that the method tends to give more consistent results when the error in the FEM is of a local nature.

The second basic approach to system identification is to determine corrections to the input parameters of the finite-element model directly so that it predicts the test modal parameters more accurately. Several automated methods have been developed for determining the effects of model input parameter changes on the analytical modal parameters using linear perturbation[15,16] and design sensitivity[17,18] methods. A method using design sensitivity and optimization techniques, presented in Refs. 1 and 2, was used in the correlation of the center segments.

Using this approach, there are two steps in the model correction process. The first step computes the design sensitivity coefficients Ω_{ij} defined as the change in state variable Ψ_i due to a change in the normalized design variable B_j. A design sensitivity coefficient represents a slope of the state variable surface in the n dimensional design variable space and can be expressed as

$$\Omega_{ij} = \frac{\partial \Psi_i}{\partial B_j} \tag{2}$$

The state variables represent the FEM modal parameters: frequency or mode shapes. The normalized design variables represent the FEM input parameters such as element material and physical properties. Several general-purpose structural analysis programs such as MSC/NASTRAN, ANSYS, and SDRC OPTISEN possess design sensitivity capability. The present analysis used MSC/NASTRAN[18] to compute the required design sensitivity coefficients.

Based on the design sensitivity coefficients, we can compute the change in the ith state variable due to small changes in the selected FEM design variables. In this work, only modal frequencies were used as state variables. To the first order, the change in frequency is therefore given by

$$\Delta\omega_i = \sum_{j=1}^{n} \Omega_{ij} \Delta B_j \tag{3}$$

Equation (2) is valid within the limits of linear perturbation theory, where the definition of a small change in the design variable is a function of the linearity of the finite-element model. Required analytical frequency corrections are determined by matching test modes and analytical modes. This is most easily done by computing cross orthogonality between the two mode sets with respect to the TAM mass matrix generated during the pretest analysis.

Unfortunately, there is not a unique set of design variable changes that will produce the desired frequency correction. Therefore, the second step in the model correction process is to determine an optimum set of model parameter corrections. Here we define optimum as a set of corrections that minimizes both the test-analysis frequency error and the required corrections to the model. We must therefore assume that the original FEM is close to the correct solution.

The optimum corrections are determined by minimizing a performance index J, which can be expressed as

$$J = (J_\Psi + J_B) \tag{4}$$

where J_Ψ is the portion of the performance index used to minimize the frequency error given by

$$J_\Psi = W_\Psi \sum_{i=1}^{m} W_{\Psi i} \, |\omega_{Ti} - \omega_{Ai}| \tag{5}$$

in which ω_{Ti} represents the test mode frequency and ω_{Ai} is the corresponding analysis frequency. The term J_B is the portion of the performance index that is used to minimize the FEM corrections given by

$$J_B = W_B \sum_{i=1}^{n} W_{Bi} \, |\Delta B_i| \tag{6}$$

Terms W_Ψ and W_B represent weighting coefficients that can be used to set the importance of minimizing the overall frequency error relative to minimizing the overall model change. In addition, coefficients $W_{\Psi i}$ and W_{Bi} can be used to weight the importance of individual modes and design variables.

Currently, the weighting coefficients W_Ψ and W_B are selected based on experience. Weighting coefficients $W_{\Psi i}$ and W_{Bi} should be selected based on confidence level. If the analyst is confident that the ith analytical frequency has been matched with the correct test frequency, $W_{\Psi i}$ should be large relative to weighting coefficients for other analytical frequencies for which there is less confidence. Likewise, if the analyst is confident in the value of the ith design variable, a relatively large value for the weighting coefficient W_{Bi} should be selected. A FORTRAN program has been written to process the design sensitivity coefficients and perform the required optimization analysis using one of two available methods: sequential search or maximum gradient. Details of this method of system identification can be found in Refs. 1 and 2.

The methods described possess advantages and disadvantages. The biggest disadvantage of the direct matrix identification methods is that they operate directly on the FEM mass and stiffness matrices. Although areas of stiffness or mass error are easily identified, the resulting corrections to matrix elements cannot be easily implemented in the finite-element model. In addition, to be economical, the methods must often be used on reduced mass and stiffness matrices, complicating the identification of the appropriate corrections to the analytical model. The advantage of this approach is that the analyst is not forced to choose appropriate design variables before the analysis. All of the matrix elements are allowed to vary to achieve correlation. These methods can also identify corrections in areas of the structure that are not explicitly modeled such as a joint.

The biggest disadvantage of the design sensitivity approach is that if the analyst chooses the wrong set of design variables to vary, an incorrect solution will result. Economic considerations prohibit using all model parameters as design variables. In addition, only frequencies can easily be used as state variables. The use of individual mode shape coefficients as state variables would result in a very large system identification problem, even for a modest number of mode shapes. The biggest advantage of the method is that it determines the corrections to the FEM input parameters directly, which provides easy interpretation for the analyst. As implemented, the method allows the user to update the model quickly in what is usually a small number of iterations. It is the authors' opinion that the advantages of the design sensitivity approach greatly outweigh the method's disadvantages and the advantages of the direct identification methods.

Correlation Results

Immediately following the inert segment modal survey, correlation of the inert segment FEM began using the design sensitivity and optimization approach of system identification.

Table 3 Test-analysis frequency error for pretest and postcorrelation (update 7) inert segment models

Test Frequency, Hz	Pretest model Mode	Pretest model Frequency, Hz	Pretest model %Error	Postcorrelation model Mode	Postcorrelation model Frequency, Hz	Postcorrelation model %Error	Description
2.14	2	0.95	−55.6	2	2.13	−0.5	First rigid-body pitch
3.32	4	1.49	−55.1	4	3.33	0.3	Rigid-body bounce
4.14	5	1.80	−56.5	5	4.03	−2.7	Second rigid-body pitch
5.00	6	2.27	−54.6	6	5.08	1.6	Second rigid-body roll
18.68	9	8.86	−52.5	9	19.02	1.8	Case-propellant forward ovaling
18.81	7	8.58	−54.4	7	18.46	−1.9	Case-propellant aft ovaling
28.98	20	23.23	−19.8	11	31.96	10.3	Case-propellant saddle
40.87	13	18.16	−55.6	15	38.70	−5.3	Case-propellant forward triangular
41.52	19	20.71	−50.1	21	41.59	0.2	Propellant
42.49	15	19.71	−53.6	21	41.59	−2.1	Case-propellant bending

Table 4 Test-analysis cross orthogonality (CGM) for postcorrelation (update 7) inert segment model

Test frequency, Hz	Postcorrelation model Mode	Postcorrelation model Frequency, Hz	CGM	Coupling	Description
2.14	2	2.13	0.98	0.15 (5)[a]	First rigid-body pitch
3.32	4	3.33	0.99	0.11 (5)	Rigid-body bounce
4.14	5	4.03	1.00	0.05 (6)	Second rigid-body pitch
5.00	6	5.08	0.99	0.09 (4)	Second rigid-body roll
18.68	9	19.02	0.92	0.30 (7)	Case-propellant forward ovaling
18.81	7	18.46	0.92	0.22(10)	Case-propellant aft ovaling
28.98	11	31.96	0.95	0.17(21)	Case-propellant saddle
40.87	15	38.70	0.63	0.48(21)	Case-propellant forward triangular
41.52	21	41.59	0.57	0.47(19)	Propellant
42.49	21	41.59	0.46	0.55 (5)	Case-propellant bending

[a]Parentheses denote corresponding analytical mode.

Table 5 Comparison of FEM physical and material properties for inert pretest, update 4, and update 7 models

Property description	Pretest	Update 4	Update 7
Motor casing thickness	0.480	0.480	0.480 in.
Motor casing elastic modulus	3.0E7	3.0E7	3.0E7 psi
Forward section propellant modulus	3,000	15,120	14,000 psi
Middle section propellant modulus	3,000	15,120	14,000 psi
Aft section propellant modulus	3,000	15,120	14,000 psi
Propellant Poisson's ratio	0.490	0.490	0.490
Suspension radial stiffness	2,400	10,000	12,500 lb/in.
Suspension tangential stiffness	2,400	12,250	12,250 lb/in.
Suspension axial stiffness	2,400	12,250	12,250 lb/in.

Table 3 compares the test and pretest analytical frequencies before correlation. Frequency errors of over 50% exist in both the rigid body and the flexible modes, indicating substantial error in both the test suspension and the segment representation. The magnitude of the frequency error in the flexible modes indicated that pretest predictions of the propellant modulus were substantially in error. Based on element strain energy distributions, design variables that could possibly account for the frequency discrepancies were selected from the model input parameters. The selected design variables included motor case thickness, propellant modulus, test suspension stiffness, factory joint properties, and field joint properties.

Each iteration, or update, of the model included a test-analysis correlation of the current model to match test and analysis mode shapes using cross orthogonality, a design sensitivity analysis to compute the design sensitivity coefficients, and optimization analysis using a special purpose FORTRAN program to identify optimum model corrections, the correction of the current model, and, finally, a modal analysis of the updated model. After several such iterations the frequency errors were substantially reduced, as listed in the postcorrelation results in Table 3. Table 4 presents the cross-orthogonality results for the final update. The four rigid-body modes are correlated in both frequency and shape, indicating that the test suspension is accurately represented in the FEM. The forward and aft ovaling modes were also accurately predicted by the updated model in both frequency and shape. The shape of the saddle mode was accurately predicted, but the corresponding analytical frequency was in error by 10.0%.

Table 5 presents important FEM input parameters for the pretest model, intermediate model update 4, and the final model update 7. The stiffness of the suspension springs had to be increased substantially in order to match the test data. This was not too surprising because no stiffness data for the airbags was available from the manufacturers. Crude tests were performed to determine approximate stiffnesses for use in the pretest FEM. The required 467.0% increase in the propellant grain elastic modulus was quite surprising. If the propellant was in fact as stiff as the modal survey and subsequent correlation analysis indicated, the methods and results of the subscale propellant tests must be reviewed. A relation between the propellant properties measured during subscale tests and the properties measured during the modal survey would have to be determined. Of all the possible design variables selected from the FEM, only the propellant elastic modulus had enough influence on the modal frequencies to account for the discrepancies between the pretest model and the test results.

The live center segment modal survey and correlation analysis immediately followed the analysis of the inert segment. Table 6 compares the pretest modal frequencies with the corresponding test data. As in the case of the inert segment, the large discrepancies in frequency indicate that the modulus of the live propellant is also much greater than that predicted by subscale testing. After initial updates of the live segment model, it was found that the most striking difference between test and analysis results was a 2.1-Hz frequency shift between the forward and aft ovaling modes in the test data. There should be a frequency difference due to the asymmetry of the

Table 6 Test-analysis frequency error for pretest and postcorrelation (update 3/5) live segment models

Test frequency, Hz	Pretest model Mode	Pretest model Frequency, Hz	Pretest model %Error	Postcorrelation model Mode	Postcorrelation model Frequency, Hz	Postcorrelation model %Error	Description
1.94	2	0.94	−51.5	2	1.96	1.0	First rigid-body pitch
3.20	4	1.47	−54.1	4	3.07	−4.1	Rigid-body bounce
3.76	5	1.79	−52.4	5	3.79	0.8	Second rigid-body pitch
4.75	6	2.25	−52.6	6	4.78	0.6	Second rigid-body roll
14.65	9	5.30	−63.8	7	14.76	0.8	Case-propellant forward ovaling
16.73	7	5.11	−69.5	9	16.58	−0.9	Case-propellant aft ovaling
28.16	29	15.16	−46.2	11	29.14	3.5	Case-propellant saddle
29.13	30	15.16	−48.0	12	29.16	0.1	Case-propellant saddle
38.63	13	10.89	−71.8	20	36.66	−5.1	Case-propellant forward triangular
40.16	12	10.51	−73.8	24	41.04	2.2	Case-propellant second-order saddle
44.71	43	17.08	−61.8	33	48.80	9.1	Case-propellant bending

Table 7 Comparison of FEM physical and material properties for live pretest, update 1, update 3, and update 5 models

Property description	Pretest	Update 1	Update 3	Update 5
Motor casing thickness	0.480	0.480	0.459	0.459 in.
Motor casing elastic modulus	3.0E7	3.0E7	3.0E7	3.0E7 psi
Forward section propellant modulus	1,000	8,900	8,000	9,612 psi
Middle section propellant modulus	1,000	8,900	8,900	11,125 psi
Aft section propellant modulus	1,000	8,900	12,150	15,792 psi
Propellant Poisson's ratio	0.490	0.490	0.490	0.490
Suspension radial stiffness	2,400	10,000	10,000	10,000 lb/in.
Suspension tangential stiffness	2,400	12,250	10,900	10,900 lb/in.
Suspension axial stiffness	2,400	12,250	10,900	10,900 lb/in.

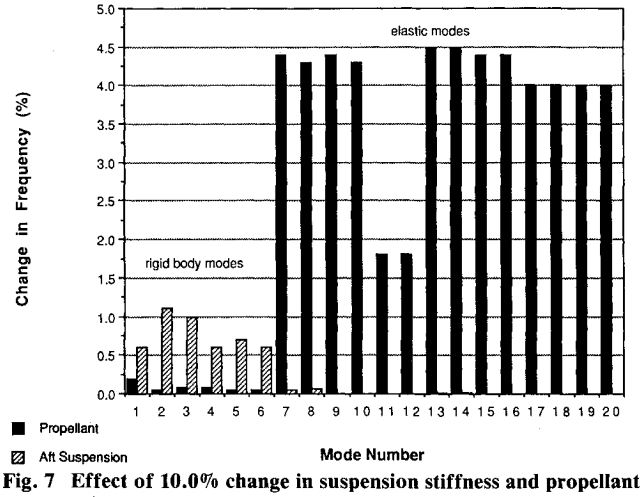

Fig. 7 Effect of 10.0% change in suspension stiffness and propellant modulus for live center segment analytical modes.

propellant bore with respect to the segment longitudinal axis, but analysis consistently predicted the aft ovaling mode approximately 0.40 Hz lower than the forward ovaling mode.

Initially, it was suspected that the test suspension was to blame for the observed frequency shift. However, the frequency separation was not observed in the inert segment test data, and the segments were positioned identically in the suspension in both tests. A design sensitivity analysis was performed to see whether a change in the radial stiffness of the suspension springs of the aft chock relative to the other suspension springs could account for the observed frequency separation. Figure 7 illustrates the percentage change in frequency in each of the first 20 analytical mode shapes due to a 10% change in the suspension stiffness. As expected, the stiffness substantially affects the rigid-body modes. However, the suspension has virtually no effect on the elastic ovaling modes and therefore would not be able to account for the frequency separation in the test data.

As stated earlier, the elastic modulus of the propellant has a profound impact on the segment elastic modes. The effect of a 10% change in the propellant modulus on the analytical frequencies is also illustrated in Fig. 7. After several updates, the frequency separation was predicted in the analytical model by dividing the propellant into three sections along the longitudinal axis and allowing the optimization routine to adjust the propellant modulus of each section. Results indicated that the aft section of propellant was stiffer than the middle section, which was then slightly stiffer than the forward section. All model iterations indicated that a stiffness gradient through the length of the propellant was the cause of the observed frequency separation. Three sections were used only because the model could be conveniently subdivided in this manner. If the stiffness gradient actually exists, it would most likely be much more complicated, requiring many subsections of propellant.

The modal frequencies of the FEM after correlation are compared to the test frequencies in Table 6. Important FEM properties are compared for the pretest model, update 1, update 3, and update 5 in Table 7. No discernible dependence of propellant modulus on frequency was observed in the correlation of the inert segment. However, in the case of the live segment, update 3 gave the best results for both frequency and mode shape for the first seven test modes, whereas the propellant had to be further stiffened in update 5 to predict the second order saddle test mode accurately. Table 6 therefore presents the test-analysis frequency comparison for updates 3 and 5 combined. The combined cross-orthogonality results for updates 3 and 5 are presented in Table 8. Eight of the test modes possess frequency errors less than 4.0% and cross-generalized mass values greater than 0.90, indicating a good overall representation of the test suspension and the live center segment. Frequency error vs model update is illustrated in Fig. 8. The design sensitivity and optimization approach of system identification resulted in a correlated model in relatively few iterations.

The objective of the modal surveys was to characterize the dynamic properties of the propellant grain. Although no pure

Table 8 Combined test-analysis cross orthogonality (CGM) for postcorrelation update 3 and update 5 live segment models

Test frequency, Hz	Postcorrelation model Mode	Frequency, Hz	CGM	Coupling	Description
1.94	2	1.96	0.99	0.11 (1)[a]	First rigid-body pitch
3.20	4	3.07	0.99	0.10 (6)	Rigid-body bounce
3.76	5	3.79	0.97	0.25 (2)	Second rigid-body pitch
4.75	6	4.78	1.00	0.03 (7)	Second rigid-body roll
14.65	7	14.76	0.96	0.21 (9)	Case-propellant forward ovaling
16.73	9	16.58	0.99	0.09 (7)	Case-propellant aft ovaling
28.16	11	29.14	0.97	0.15(13)	Case-propellant saddle
29.13	12	29.16	0.73	0.51(13)	Case-propellant saddle
38.63	20	36.66	0.42	0.36(38)	Case-propellant forward triangular
40.16	24	41.04	0.91	0.25(38)	Case-propellant second-order saddle
44.71	33	48.80	0.42	0.39(37)	Case-propellant bending

[a]Parentheses denote corresponding analytical mode.

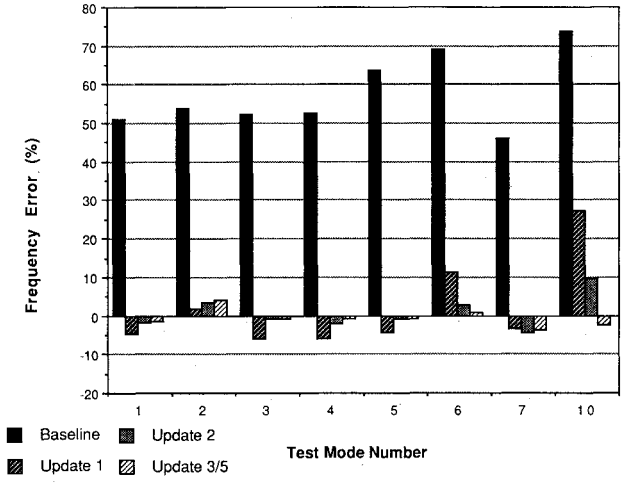

Fig. 8 Test-analysis frequency error for live center segment.

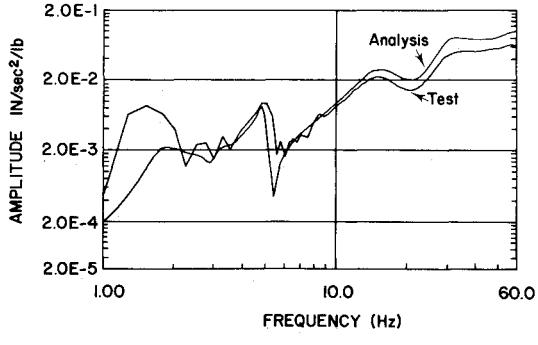

Fig. 9 Comparison of test and analysis radial response at center segment forward end due to oblique input at forward end.

propellant modes were correlated between test and analysis, four case-propellant modes that are dominated by the elastic modulus of the propellant were accurately predicted by the final updated model. Several other modes predicted by the analytical model were not identified in the test data; however, a comparison of test and analysis frequency response functions shows that the final updated model does accurately represent the test article. Figure 9 compares test and analysis frequency response functions between an oblique input at the forward end of the segment and a radial response on the case, also near the forward end.

Although the reasons for the propellant modulus discrepancy between subscale testing (RDS) and the modal survey test results are still under investigation, further RDS testing and literature review have uncovered some possible explana-

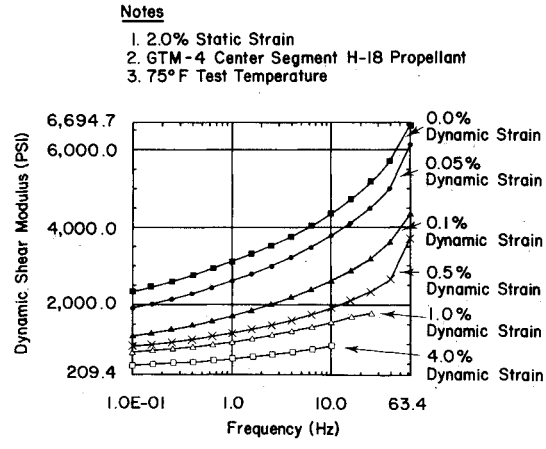

Fig. 10 Rheometric dynamic spectrometer test data for inert propellant.

tions. The propellant dynamic modulus can vary with temperature, static strain or preload, and dynamic strain or excitation amplitude. Dynamic modulus has been observed to increase with decreasing temperature, increasing excitation frequency, increasing static strain, and decreasing dynamic strain.[19-21] After the modal surveys, it was discovered that the dynamic strain level applied to the RDS test specimen could dramatically affect the dynamic modulus of the propellant. The RDS test was altered so that both the static and dynamic shear strains applied to the test specimen would be more consistent with the modal survey conditions.

Figure 10 illustrates typical RDS data for inert H-18 propellant plotted to display the effect of varying dynamic strain level. During the inert segment modal survey, maximum dynamic shear strains were on the order of 0.01%. Combining this level of dynamic strain with a frequency of approximately 20.0 Hz would yield a value of dynamic shear modulus from Fig. 10 between 4500 and 5000 psi, assuming a static strain of 2.0%. The corresponding elastic modulus would be between 13,500 and 15,000 psi. The value of 14,000 psi predicted in the inert segment correlation analysis compares very well with these new subscale test results. The pretest elastic modulus value of 3000 psi was obtained from aged inert specimens in which the static strain was zero and the dynamic strain was 2.0%. This value of modulus also compares favorably with the results of Fig. 10. The strain levels used in pretest analysis were historically consistent with older dynamic modulus test procedures.

Currently, investigations are being planned to explore the relationship between the results of RDS and other forms of subscale testing and the results of the modal surveys. Once the

principles behind the relationship are better understood, it is hoped that the same principles can be extended to propellant dynamic modulus characterization of Shuttle liftoff and flight events based on subscale testing results.

Conclusions

Modal surveys of inert and live Shuttle SRB center segments in a simulated free-free state were performed to characterize the dynamic properties of the solid propellant grain. Advanced pretest analysis techniques were used to determine accelerometer locations and generate an exact reduced representation of the FEM called a TAM for use in test-analysis correlation. Following the modal surveys, the analytical models were rapidly updated using design sensitivity and optimization techniques resulting in analytical representations that accurately predicted the test data.

Large test-analysis frequency discrepancies were found for both of the pretest segment models. To correlate the inert FEM with its corresponding test data, the propellant elastic modulus had to be increased by a factor of 4.67 over the value originally predicted by RDS testing before the modal test. Increasing the suspension stiffnesses resulted in accurate prediction of the test rigid body modes, indicating an accurate analytical representation of the test suspension. Many FEM parameters were considered as design variables; however, only propellant modulus was able to account for the large frequency errors without making physically unrealistic model changes.

In addition to a large increase in the value of the propellant elastic modulus, a longitudinal propellant modulus gradient was required in the live segment to accurately predict a 2.1-Hz frequency separation between the forward and aft ovaling modes in the test data. Although a modulus gradient was the only physically realistic way to account for the frequency shift, other unmodeled or unknown phenomena could be present. Currently, there is no physical explanation regarding why a longitudinal gradient would appear in the propellant stiffness. Further testing and analysis have been suggested in an attempt to identify and clarify the exact cause of the observed frequency separation.

The results of the test-analysis correlation showed that care must be taken to measure the propellant dynamic properties in such a way that they are consistent with the static and dynamic loading for which the modulus is needed. That is, the RDS specimens must be subjected to both static and dynamic strain levels that are characteristic of the modal survey or other dynamic event being simulated. Since the modal surveys and correlation analysis, further subscale testing was performed at dynamic strain levels consistent with modal survey levels. The results of the new RDS testing are consistent with the values of propellant elastic modulus determined from the modal survey.

References

[1]Flanigan, C. C., "Test/Analysis Correlation of the STS Centaur Using Design Sensitivity and Optimization Methods," *5th International Modal Analysis Conference,* Union College, Schenectady, NY, April 1987, pp. 99-107.

[2]Flanigan, C. C., "Test/Analysis Correlation Using Design Sensitivity and Optimization," Society of Automotive Engineers, TP-871743, Warrendale, PA, 1967.

[3]"The Analysis of Nearly Incompressible Materials with the HEXA (8) Element," NASTRAN Application Note—April 1982, *MSC/NASTRAN Application Manual,* Vol. I, MacNeal-Schwendler Corp., Los Angeles, CA.

[4]Kammer, D. C., Flanigan, C. C., and Dreyer, W., "A Superelement Approach to Test-Analysis Model Development," *4th International Modal Analysis Conference,* Union College, Schenectady, NY, Feb. 1986, pp. 663-673.

[5]Kammer, D. C., "Test-Analysis Model Development Using an Exact Modal Reduction," *International Journal of Analytical and Experimental Modal Analysis,* Vol. 2, Oct. 1987, pp. 174-179.

[6]Hunt, D. L. and Peterson, E. L., "Multishaker Broadband Excitation for Experimental Modal Analysis," Society of Automotive Engineers Paper 831435, Warrendale, PA, 1985.

[7]Williams, R. and Vold, H., "Multiphase-Step-Sine Method for Experimental Modal Analysis," *International Journal of Analytical and Experimental Modal Analysis,* Vol. 1, No. 1, April 1986, pp. 25-34.

[8]Leuridan, J. M. and Kundrat, J. A., "Advanced Matrix Methods for Experimental Modal Analysis—A Multi-Matrix Method for Direct Parameter Extraction," *1st International Modal Analysis Conference,* Union College, Schenectady, NY, Nov. 1982, pp. 192-200.

[9]Brillhart, R., Hunt, D. L., Kammer, D. C., Jensen, B. M., and Mason, D. R., "Modal Survey and Test-Analysis Correlation of the Space Shuttle SRM," *6th International Modal Analysis Conference,* Union College, Schenectady, NY, Feb. 1988, pp. 863-870.

[10]Baruch, M. and Bar Itzhack, I. Y., "Optimal Weighted Orthogonalization of Measured Modes," *AIAA Journal,* Vol. 16, April 1978, pp. 346-351.

[11]Berman, A., "Mass Matrix Correction Using an Incomplete Set of Measured Modes," *AIAA Journal,* Vol. 17, Oct. 1979, pp. 1147-1148.

[12]Berman, A., Wei, F., and Rao, K. V., "Improvement of Analytical Dynamic Models Using Modal Test Data," *21st AIAA Structures, Structural Dynamics, and Materials Conference,* AIAA, New York, 1980, pp. 809-814; also AIAA Paper 80-0800, May 1980.

[13]Kabe, A., "Stiffness Matrix Adjustment Using Mode Data," *AIAA Journal,* Vol. 23, No. 9, Sept. 1985, pp. 1431-1436.

[14]Kammer, D. C., "An Optimum Approximation for Residual Stiffness in Linear System Identification," *AIAA Journal,* Vol. 26, Jan. 1988, pp. 104-112.

[15]Garba, J. A. and Wada, B. K., "Applications of Perturbation Methods to Improve Analytical Model Correlation with Test Data," Society of Automotive Engineers, TP-770959, Warrendale, PA, Nov. 1977.

[16]Chen, J. C. and Garba, J. A., "Analytical Model Improvement Using Modal Test Results," *AIAA Journal,* Vol. 18, June 1980, pp. 684-690.

[17]Collins, J. D., Hart, G. C., Hasselman, T. K., and Kennedy, B., "Statistical Identification of Structures," *AIAA Journal,* Vol. 12, Feb. 1974, pp. 185-190.

[18]"Design Sensitivity Analysis," *MSC/NASTRAN Application Manual,* Vol. I, MacNeal-Schwendler Corp., Los Angeles, CA.

[19]Hufferd, W. L., "Dynamic Characterization and Analysis of Space Shuttle SRM Solid Propellant," NASA Contract NAS8-32234, April 1987.

[20]Cole, J. E., "The Effects of Frequency, Amplitude, and Load on the Dynamic Properties of Elastomers," Office of Naval Research, Contract N00014-69-C-0056, Aug. 1965.

[21]Hobaica, E. C. and Sweet, G., "Behavior of Elastometric Materials Under Dynamic Loads," *Shock and Vibration Digest,* Vol. 8, March 1976, pp. 77-88.